Egyptian Journal of Chemistry

http://ejchem.journals.ekb.eg/

Corrosion and Characterization of Ni-Cu Deposited Layer on 304 Alloy

Y. Reda

Chemical Engineering Department, Canal High Institute of Engineering and Technology, Suez, Egypt

Abstract

The major goal of this study is to see how time depositing affects the surface characteristics, composition, and corrosion behaviour of Ni–Cu NMFs that have been deposited. The deposited layer's Ni content ranged from 76 to 85 percent, with copper content ranging from 10 to 19 percent. Potentiodynamic tests, CV, and EIS were used to investigate the corrosion behaviour of these deposited Ni-Cu in 1 M acidic methanol. A typical dendritic morphology was developed using a high current density of 3A/〖cm〗^2 and different deposition times of 30, 90, and 150 sec. The layer deposited at 30 seconds had the lowest corrosion rate of 25.3 mpy, according to the potentiodynamic test. According to CV, when the deposition period rises from 30-150 sec, both the overall charge and forward peak intensity are increasing, indicating a considerable influence on the films' electrochemical activity. The author analysed Rpo to decrease as the applied electrodeposition time increased in the EIS test. At 30 sec, the maximum Rpo was 442.6 ohm, indicating the best corrosion resistance.

Keywords: Microstructure; Corrosion; Nanostructure metallic foams (NMFs); cyclic voltammetry (CV); EDX; polarization resistance (R_{po}); Linear scan voltammetry (LSV); Hydrogen Bubble Dynamic Template (DHBT); Nanoporous Metallic Foams (NMFs).

1. Introduction

A high specific area, mechanical strength, fluid permeability, shape-selective effects, chemical, and thermal stability are the most essential qualities for Nanoporous materials [1]. Mechanical characteristics and high electrical conductivity are two of the most important qualities of porous metals [2]. Template synthesis [3-5], surfactant-mediated synthesis [6-7], and dealloying [8] are all approaches for making nanoporous metals. DHBT Electrodeposition techniques are utilized to create materials with unique forms and morphologies that are impossible to achieve by other approaches [9]. DHBT develops porous materials for sensing [10-11], catalysis [12], and energy [13]. Copper is used due to its excellent electrical and thermal conductivity, as well as its resistance to corrosion. Nickel is robust, has good corrosion and oxidation resistance, and has high strength at high temperatures. [14-15]. The production of Hydrogen bubbles on the substrate precludes metal deposition in the gaped area in this approach. The metal ions from a foam structure between the gas bubbles during hydrogen evaluation, and hydrogen behaves as a negative dynamic template [16-17]. Single metals, such as silver, gold, and palladium [18-20], as well as a variety of bimetallic complexes, such as AuPt, AgPd, and NiCu[21-23], can be produced using this process. The manufacture of NMFs was done by cathodic electrodeposition with DHBT [24]. When operating beyond existing densities of 1 A/cm^2 on St. St. substrates, porous Ni–Cu metallic foams reveal a dendritic topology. [25] employed a hydrogen bubble template to create Ni-Cu NMFs with both Ni- and Cu-rich phases by electrodeposition. In the hydrogen bubbles left the area, Ni-Cu NMFs porous films with Nano dendritic walls were deposited. This study compares the effects of changing the deposition time at a steady current on the form, chemical content, and corrosion behaviour of NMFs deposited by the DHBT approach with prior studies.

Materials and Methods

2.1 Synthesis of Cu – Ni MMFs

In the deposition process, stainless steel 304 specimens with dimensions of 4 x 1.5 cm x 0.4 mm were employed. The chemical composition of St. St. 304 is shown in Table 1. Before electrolytic activation in 37 percent HCl at room temperature, all specimens were washed with acetone solvent and rinsed with distilled water to eliminate any leftover activation chemicals. The positive electrode was made of graphite. Using a power supply 6200 P&H soft panel, a high current density of 3A/cm^2 was used for Cu–Ni NMFs electrodeposition with deposition times of 30, 90, and 150 sec. The operating

*Corresponding author e-mail: ysyy5@hotmail.com.; (Y.Reda).
Receive Date: 04 February 2022; Revise Date: 18 February 2022; Accept Date: 28 February 2022.
DOI: 10.21608/EJCHEM.2022.120079.5389.

conditions and bath composition are shown in Table 2.

Table 1;Chemical composition of St. St. 304

Element	C	N	Si	V	Cr	Mn	Co	Ni	Fe
wt.%	0.04343	0.01661	0.53366	0.12499	18.53794	1.00484	0.18672	8.10927	Rem.

Table 2; Electrolytic bath composition and electrodeposition working conditions.

Chemical bath Composition	
$NiSO_4.6H_2O$	0.5 M
H_2SO_4	1 M
HCl	0.05 M
H_3BO_3	0.1 M
$CuSO_4.5H_2O$	0.01 M
sodium citrate tribasic dehydrate	0.2 M
Working Conditions	
Time (sec)	30, 90, 150
Current density (A/cm^2)	3
pH	0. 7 reach 1
Temp.,^{0}C	50

2.2 Characterization

2.2.1 surface morphology and chemical analysis

The morphology and chemical analyses of the deposited Ni-Cu layers were examined using an SEM attached to an EDX unit (Model Quanta 250 FEG), with an accelerating voltage of 30 KV.

2.2.2 Electrochemical measurements

Using a PAR 273A potentiostat and Power Suite software, electrochemical experiments were performed in a 125 mL beaker. The working electrode was a Ni–Cu foam deposited layer, with a Pt electrode serving as a counter electrode and an Ag/Ag Cl electrode serving as a reference electrode. For the looks like fuel cell test, 1 M Methanol + 0.5M H_2SO_4 solutions were used. At a scan rate 0.5 mV S1, at 25 ^{0}C, LSV measurements were utilized to scan the electrode potential from the open circuit potential (OCP, ca. -0.035 V) to -0.335 V vs. SCE. A potential of -0.185 V vs. SCE was applied for 15 minutes before the test to remove any oxides on the surface. The excitation signal was a 10 mV peak-to-peak sine wave with an AC frequency range of 0.1–105 Hz. At E_{corr}, electrochemical impedance spectra (EIS) were recorded.

2. Results and Discussion

3.1 Surface Characterization:

Figure 1 shows SEM pictures of Ni-Cu electrodeposited layers after deposition times of 30, 90, and 150 sec with a current density of 3 A/cm^2 and morphological analysis. The deposited layers have a typical dendritic shape to them. The porous structure and dendritic walls were formed in all circumstances, as shown in Figures 1(a-c). Figure 1a depicts the appearance of the dendritic structure after 30 sec of deposition. he deposition time increases, the electrodeposition process becomes mass transfer regulated, and dendritic growth and density get denser, particularly at deposition times of 90 and 150 sec (Fig. 1.b-c). In the DHBT process, the cathodic reaction occurs when metal ions in the electrolyte are reduced to H+, resulting in the formation of porous and high-surface-area films [26-28].

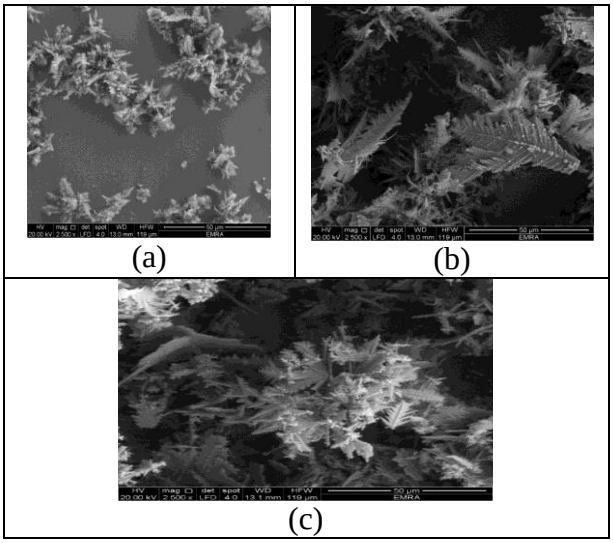

Fig. 1: SEM of Ni–Cu foams deposited at 3 A cm^{-2} for deposition time, a) 30sec, b) 90sec, and 150 sec .

Figures 1 (b-c) demonstrate a dense surface pore area that grows as deposition time goes on. The density of surface pores reduces as the deposition period increases, and the pore size of the Ni–Cu foams increases, as illustrated in Fig. 1.a. The morphology displays a large concentration of Ni at the pores' inner walls, whereas Cu forms the porous skeleton. Ni is a 'negative duplicate' of the Cu framework in several ways [25]. A phenomenon of bubble break-off diameter occurred in the solution because of the large overpotential utilized by DHBT, resulting in the bubbles' nucleation on the surface due to the saturation of H_2 at the electrode. Small bubbles continue to appear as they attach to the surface, becoming larger until a crucial size is reached. The process was triggered by a bubble's capacity to form

a single group and its relaxation time on the surface, which is determined by its energy and the shape of the surface where lowering happens [29-30]. The serial metal ions' CO reduction in the similar electrolyte affects the bubbles. These bubbles have a direct impact on the metal deposition process. To drive the ions to find a way around the bubbles, hydrogen bubbles blocked the substrate surface, lowering the incoming metal ions [30].

The bubble detaches itself from its deposited location on the surface, resulting in a void. The thickness and size of the metal film increase with increasing deposition time, with relatively tiny pore diameters near the film surface, which increases progressively in a pileup [31]. At greater current densities, the morphology of metal foams leads to grain refinement and a drop in the lattice parameter. When working at a high density of the current, a significant quantity of clustered hydrogen bubbles occurs, preventing metal atoms from expanding in the direction of the hydrogen bubbles. Deposition takes place within the pores of hydrogen bubbles, forming a porous electrodeposition structure [30]. When the time of deposition is extended, hydrogen bubbles form in the deposited Ni– Cu film as well as on the steel surface, obstructing the diffusion control required for dendritic growth. Figure 2 shows the EDX analysis of the deposited specimens' chemical composition. As shown in Table 3, the chemical composition of the specimen at 3 A/cm^2 indicates the presence of Ni, Cu, and oxygen. Ni concentrations ranged from 76.03 to 85.09 percent, copper concentrations from 10.5 to 19.35 percent, and oxygen concentrations from 1.32 to 3.75 percent.

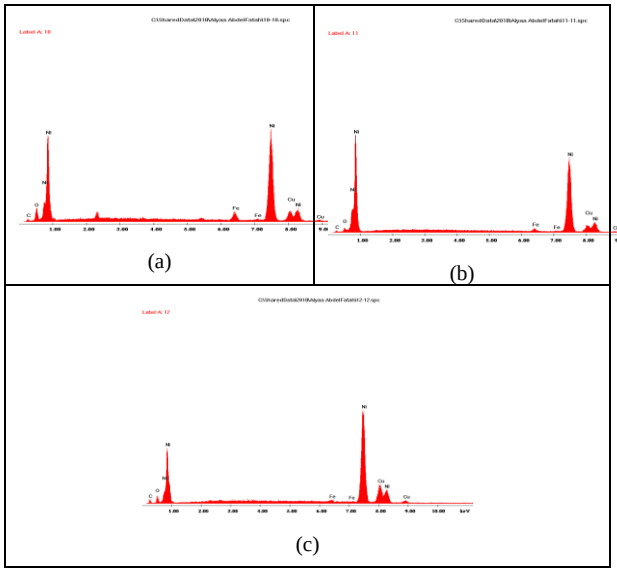

Fig. 2: EDX of Ni–Cu foams deposited at 3 A cm^{-2} at different time a) 30, b) 90, and c) 150 sec

Table 3: EDX Chemical analysis of Ni-Cu electrodeposited layers

%Element	30 sec	90 sec	150 sec
Ni	79.49%	85.09%	76.03%
Cu	11.75%	10.5%	19.35%
O	3.75%	1.32%	1.35%

3.2 Corrosion tests:

3.2.1 Potentiodynamic Polarization Test

The corrosion behaviour of electrodeposited Ni-Cu metallic foams in 1 M Methanol+ 0.5M H_2SO_4 as a function of the time of deposition is depicted in Figure 3.a. Table 4 includes all corrosion data, including corrosion current, potential, rate, and Tafel's constants for cathodic and anodic corrosion. Porous Ni-Cu layers electrodeposited at a current density of 3 A/cm^2 for 30 sec had the lowest corrosion rate (25.3 mpy).

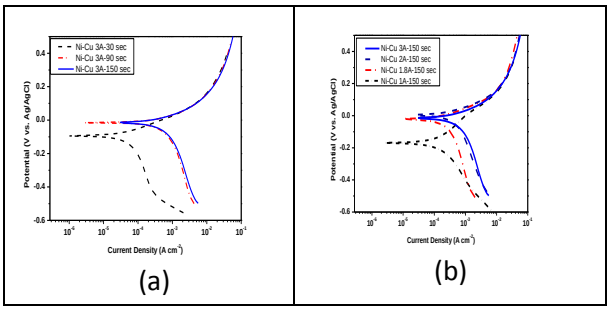

Fig. 3: Polarization curves for the corrosion of Ni/Cu foam, a) current density 3 A/cm^2 for deposition time (30-90-150 sec) ,b) current densities 1-1.8-2 &3 A/cm^2 (150 sec) in 0.5M H_2SO_4 + 1M C_2H_5OH at 25°C[34-35]

The specimen with the highest corrosion current (48.9 µA/cm^2) was chosen. While porous Ni-Cu layers electrodeposited at a current density of 3 A/cm^2 for 150 sec had the highest corrosion rate (426.8 mpy). The highest corrosion current (824 µA /cm^2) accompanied this. This stratum contained 76.03 percent Ni, 19.35 percent Cu, and 1.35 percent O, according to EDX analysis. According to the SEM, the surface form was characterized by the creation of an extraordinarily thick dendritic structure. Metal ions move from the metal surface into solution in acidic conditions, suggesting anodic corrosion, whereas hydrogen ions discharge generate hydrogen gas and reduce oxygen, showing cathodic corrosion [32].

The Tafel slopes c range from 396 to 653 mV dec-1, as shown in Table 4. According to the slopes of Tafel of roughly 120 mV dec-1, the Volmer step – which corresponds to hydrogen electrochemical adsorption in the surface of the electrode – is the rate-determining phase of the hydrogen evolution reaction "HER" at the electrodes in the foam [33-34].

The βc values obtained are significantly greater than those found in Ni-Cu thin film deposits studied in 1 M Methanol + 0.5M H_2SO_4 [35-36]. By comparing the results obtained at the greatest corrosion rate at

deposition time 150sec to our earlier study [37] for different current density ranges (1, 1.8, 2 A/cm^2) at 150sec. Figure 3.b and Table 5 show the results of the comparison. This comparison revealed that the value of this worked piece is consistent with earlier research, suggesting that corrosion rate increases as deposition time increases at any current density. At the maximum current density (3A/cm^2), the highest corrosion rate (426.8 mpy) was recorded.

Table 4: Polarization data for the corrosion of Ni/Cu foam at 3 A/cm^2 (30-90-150 sec) in 0.5M H_2SO_4 + 1M C_2H_5OH at 25°C

Electrode	Ecorr. mV	Icorr. µA/cm^2	Tafel slopes		Corrosion rate (C.R.) mpy
			βa V/decade	βc V/decade	
Ni/Cu 3A-30 sec	-93.8	48.9	0.092	0.396	25.3
Ni/Cu 3A-90 sec	-15.1	727.0	0.149	0.652	376.2
Ni/Cu 3A-150 sec	-15.0	824.0	0.149	0.653	426.8

Table 5: Polarization data for the corrosion of Ni/Cu foam at(1-1.8-2 and 3) A/cm^2 and 150 sec in 0.5M H_2SO_4 + 1M C_2H_5OH at 25°C

Electrode	Ecorr. mV	Icorr. µA/cm2	Tafel slopes		Corrosion rate (C.R.) mpy
			βa V/decade	βc V/decade	
Ni/Cu 1A-150 sec	-23.6	294	0.2877	0.3638	152.4
Ni/Cu 1.8A-150 sec	-21.2	303	0.1197	0.6508	156.9
Ni/Cu 2A-150 sec	-3.6	570	0.1377	0.5988	294.9
Ni/Cu 3A-150 sec	-15	824	0.1487	0.6534	426.8

3.2.2 Cyclic Voltammetry:

Figure 4.a shows the electrochemical analysis of Ni–Cu foams in a 1 M acidic methanol solution using a CV. The presence of two peaks indicates that Ni and Cu are present. CV measures an increase in total charge and forward peak intensity as deposition time increases, which has a significant impact on the film's activity. In the potential range of -0.02 to +1.8 V, voltammograms of Ni–Cu foams show several redox peaks. When methanol is added to the electrolyte, the look of voltammograms on the electrode surface changes dramatically.

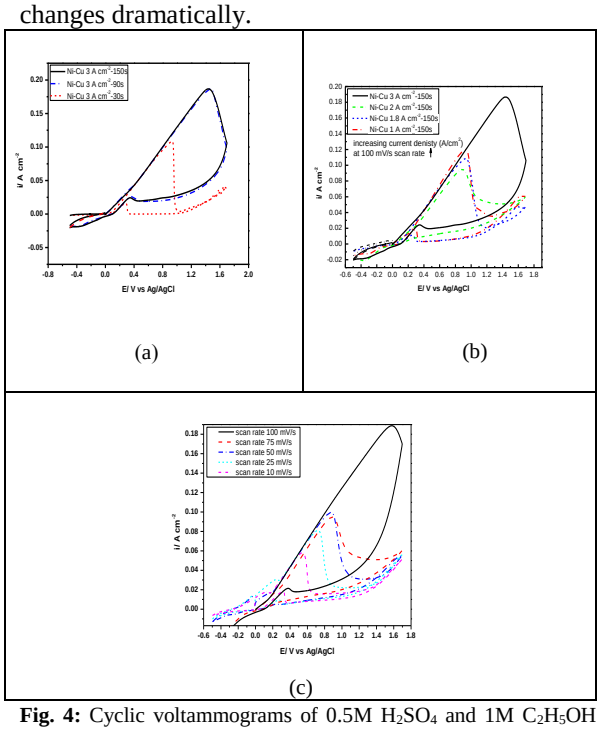

Fig. 4: Cyclic voltammograms of 0.5M H_2SO_4 and 1M C_2H_5OH solution on Ni–Cu foams a deposited at 3 A cm^{-2} ,a) different deposition times 30-90-150 sec (scan rate 100 mV s^{-1}), b) deposited at 150 sec with different deposition current densities 1-1.8-2-3 A cm^{-2} (scan rate 100 mV s^{-1}) [34-35], c) deposited at 3 A cm^{-2} with different scan rates (10-25-50-75-100 mV s^{-1}) deposition times 150 sec[34-35]

Methanol oxidation was identified in reverse (Ib) and forward (If) scans by well-separated anodic peaks. The quantity of methanol oxidized at the electrode was proportional to the magnitude of the peak in the (If) scan. The (Ib) scan was caused by the elimination of carbon monoxide (CO) and the formation of residual carbonaceous species in the (If) scan. The anodic peak is caused by methanol oxidation, whereas the cathodic peak is caused by the reaction of the reducing, according to K.Chih-Chien[38 -39]. Due to higher Methanol low theoretical oxidation potential (0.02 V) as compared with that of hydrogen (0.0 V). Consequently, each oxidized methanol molecule produces CO2 and 6 electrons, which are transmitted from the anode to the cathode through an external circuit [40]. The maximum peak intensity was observed at a scanning rate of 100 mv/sec. Figure 4.b shows a decrease in peak separation in the voltammograms as deposition time rises, as well as a broadening of the peaks. The electrolyte transport and ohmic resistance through polarization of the electrode material and the pores cause high peak separation of porous materials in the CV. Figure 4.b shows the comparison of the obtained values at deposition time 150sec with previous works [34-35] for Ni-Cu thin film deposits using different current density ranges (1,1.8,2 A/cm^2) at 150sec, while figure 4.c shows the comparison at different current density with changing scanning rate from 10-100mv/sec. This comparison revealed that the value of this worked article is consistent with prior studies, demonstrating that the

peak intensity increases with increasing deposition time at any current density, as seen in figure 4.c as the scanning rate increases. At the maximum current density (3A/cm^2), the highest peak intensity was found. The shape of voltammograms is affected by morphology and electrode porosity, according to Menshykau and Compton [41-44].

3.2.3 Electrochemical Impedance-EIS Test

The arc diameter of layers electrodeposited for a longer duration is lower in Figure 6.a, showing that they have minimal charge transfer impedance. The diameter of the lowest arc was obtained for porous Ni-Cu layers electrodeposited at 3 A/cm^2 for 150 seconds. Each electrodeposition condition's Nyquist plot is made up of two semi-circles. Table 6 summarises the results of EIS experiments performed in C2H5OH acidic solution of the examined electrocatalytic coatings at current density 3 Amp/cm2 and deposition times 30, 90, and 150 sec. Because all the specimens used the same electrolyte, the solution resistance (Rs) varied somewhat. In addition to this, the lowering polarisation resistance (R_{po}) as the electrodeposition duration increased can be seen. The lowest polarisation resistance (51.7 ohms) was found in porous Ni-Cu films electrodeposited at 3 A/cm^2 for 150 sec. Figure 5 shows the electrochemical interface equivalent circuit model that is used to represent the electrocatalytic activity of the deposited electrode, where Rsol is the solution resistance, Rp is the polarisation resistance, and Rs is the polarization resistance (Resistance are in ohm). Figure 6.b depicts Nyquist plots of 0.5M H_2SO_4 and 1M C_2H_5OH solution on deposited Ni–Cu foams at 1-1.8-2 and 3A cm^{-2} at 150sec at 25 ^oC, comparing the obtained values obtained at deposition time 150sec [34-35] with previous works for Ni-Cu thin film deposits for applying different current density ranges (1, 1.8, 2& 3 A/cm^2) at 150sec for applying different current density ranges. This comparison revealed that the value of this worked article is consistent with earlier research, suggesting that the Rp decreases as deposition time increases with increasing current density, regardless of current density.

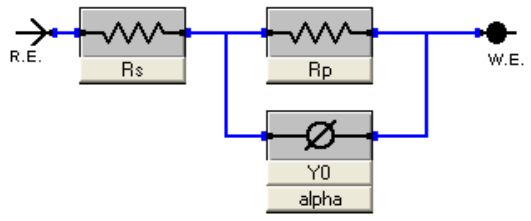

Fig.5: Equivalent circuit represents the behavior of porous Ni-Cu electrodeposited layers in 1M C_2H_5OH acidic solution at 25 ºC.

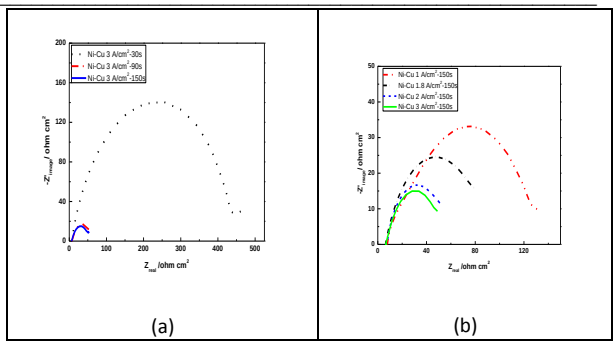

Fig. 6: Nyquist plots of 0.5M H_2SO_4 and 1M C_2H_5OH solution on Ni–Cu foams a deposited at 3 A cm^{-2} ,a) deposition times 30-90-150 sec at 25 ºC, b)deposited at 1-1.8-2 &3A cm^{-2} with deposition time 150 sec at 25 ºC[34-35]

Table 6: Equivalent circuits and specific capacitances A common feature of most of the circuit is the presence of the solution resistance (Rs), polarization resistance (Rp)

Electrode	Rp (ohms)	Rs (ohms)	alpha
Ni-Cu 3A/cm2-30 s	442.6	6.9	0.7454
Ni-Cu 3A/cm2-90 s	59.6	6.8	0.6518
Ni-Cu 3A/cm2-150 s	51.7	6.6	0.662

3. Conclusion

A typical dendritic morphology was created using a high current density of 3A/cm^2 and different deposition times of 30, 90, and 150 sec. The deposited layer's Ni concentration ranged from 76 to 85 percent, with a copper level ranging from 10 to 19 percent. The layer deposited at 30 sec had the lowest corrosion rate of 25.3 mpy, according to the potentiodynamic test. As deposition time rises, both the total charge and the forward peak intensity assessed by CV increase, demonstrating that deposition time has a major influence on the films' electrochemical activity. The Rpo decreased as the applied electrodeposition time increased in the EIS test. The greatest Rpo was 442.6 ohm after 30 sec of deposition, indicating the best corrosion resistance. Both resistance in ohms and diffusion of electrolyte through polarization of the electrode substance and the pores contribute to the significant peak divergence of porous materials in cyclic voltammograms.

5. Conflicts of interest

"There are no conflicts to declare".

6. Formatting of funding sources

This paper is funded as a project of Cairo University

7. Acknowledgments

Thanks for all team of Corrosion and Surface Treatment Lab, Cairo University

8. References:

[1] T. Jibowu, Front Nanosci Nanotech. 2(4) (2016) 165-168.

[2] A. Mathur, J. Erlebacher, Appl. Phys. Lett. 90 (2007) 061910 -061913.

[3] J. Snyder, P. Asanithi, A. B. Dalton, J. Erlebacher, Adv. Mater. 20 (2008) 4883-4886.
[4] D. Mott, J. Luo, P. N. Njoki, Y. Lin, L. Wang, C. J. Zhong, Catal. Today. 122 (2007) 378- 385.
[5]A. A. Vega, R. C. Newman, J. Electrochem. Soc. 161 (2014) C1- C10.
[6]A. V. Ruban, H. L. Skriver, J. K. Nørskov, Phys. Rev. B. 59 (1999) 15990-15600.
[7] L. Vitos, A. V. Ruban, H. L. Skriver, J. Kollar, Surf. Sci. 411 (1998) 186- 202.
[8] S. Nam, H. Jo, H. Choe, D. Ahn, H. Choi, Mat. Trans. 55(9) (2014) 1414-1418.
[9] J.Liu, J.Wang, F.Kong, T. Huang , A.Yu, Cataly. Commun., 73 (2016) 22-26.
[10]Y.Li, Y.Y. Song , C. Yang, X.H. Xia, Electrochem. Commun 9(5) (2007) 981-988.
[11] Y. F. Sun, S.B. Liu , F.L Meng, J.Y. Liu, Z.Jin, L.T. Kong, J.H. Liu, Sensors. 12(3) (2012) 2610-2631.
[12] C. M. A. Parlett, K. Wilson, A. F. Lee, Chem. Soc. Rev. 42(9) (2013) 3876-3893.
[13] Y. Li, Y. FuZ., B. L. Su, Adva. Functi.Mat. 22(22) (2012) 4634-4667.
[14] K. Sreekar, F. L. Frank, W. N. Joseph, Int. J. Adv. Manuf.Techn.(2019) 1-12.
[15] J. Tingzhu, Z. Weifang, L. Ning, L. Xuerong, H. Lu, D. Wei, Environ. Mat. 12 (2019) 1869.
[16] D.Hess, Proceedings of The National Conference on Undergraduate Research (NCUR) University of Kentucky, Lexington, KY (2014).
[17] C. A. Marozzi, A.C. Chialvo, Electrochimica Acta, 45(13) (2000) 2111-2120.
[18] K. Y.Chan, J. Ding, J. Ren , S. Cheng, K.Y. Tsang, J. Mat. Chem. 14(4) (2004) 505-516.
[19] B.J. Plowman, S.K. Bhargava, A.P. O'Mullane, Analyst. 136 (24) (2011) 5107-5119.
[20] G.M. Yang, X. Chen, J. Li, Z. Guo, J.H. Liu , X.J. Huang, Electrochimica Acta. 56(19) (2011) 6771-6778.
[21] J. Liu, L. Cao, Y. Xia, Z. Li, Int.J. Electrochem. Sci. 8(7) (2013) 9435-9441.
[22] J. L. Yin, J. Y. Park, Int. J. Hydrogen Energy. 39(29) (2014) 16562-16568.
[23] J. Liu, L. Cao, W. Huang, Z. Li, ACS Appl. Mat.and Interfaces. 3(9) (2011) 3552-3558.
[24] S.Euge´nio, T. M.Silva, M. J.Carmezim, J Appl Electrochem. 44 (2014) 455–465.
[25] J. Zhang, M. D. Baro, E. Pellicer, J. Sort, Nanoscale 6 (2014) 12490-12499.
[26] E. M. Fayyad, A. M. Abdullah, M. K. Hassan, A.M. Mohamed, G. Jarjoura, Z. Farhat, Emergent Mat. 1 (2018) 3–24.
[27] Lamiaa Z. Mohamed · Mohamed A. H. Gepreel · Aliaa Abdelfatah, Chemical Papers,2021 https://doi.org/10.1007/s11696-021-01791-9
[28] Aliaa Abdelfatah, Mohamed Abu-Okail, Lamiaa Z. Mohamed, Int. J. Electrochem. Sci., 16 (2021) 151001.
[29] B. J. Plowman, L. A. Jones, S. K. Bhargava, Chem.Commun.51(21) (2015) 4331-4346.
[30] V.S.Damme, P. Maciel, H. V.Parys, J. Deconinck, A.Hubin, H. Deconinck, Electrochem. Commun. 12(5) (2010) 664-667.
[31] D. K. J. Oppedisano, Ph.D., RMIT University, Melbourne (2016).
[32] J. Niu, X. Liu, K. Xia, L. Xu, Y. Xu, X. Fang, W. Lu, Int. J. Electrochem. Sci. 10 (2015) 7331-7340.
[33] Sam J., Abraham J., Sajini T., Ajith J. J., Egyptian Journal of Petroleum (2017) 26, 721–732
[34] D. M.F. Santos, S. Eugenio, C. A.C. Sequeira, M. F. Montemor, ECS Trans. 64(29) (2015) 9-16.
[35] D. M.F. Santos, S. Eugenio, C. A.C. Sequeira, M. F. Montemor, ECS Trans. 64(29) (2015) 9-16.
[36] R. Abdel-Karim, Y. Reda, K. M. Zohdy, A. Abdelfatah, S. El-Raghy, Int. J. Electrochem. Sci. 14 (2019) 3035 – 3054.
[37] Reda, Y., Abdel-Karim, R., Zohdy, K.M., S.M. Ain Shams Engineering Journal, (2021) online 13 july
[38] K. Chih-Chien, L. Po-Yuan, X. Yuhua, A. Rohan, D. Liming, Y. Xiong, L. Chung-Chiun, J. Power Sources 256 (2014) 329-335.
[39] S. Mohan, S.O. Bade Shrestha, The Open Fuels & Ener. Sci. J. 2 (2009) 124-128.
[40] S.S.Gupta, S.Singh, J.Datta, Mater. Chem. Phys.. 116 (2009) 223-228.
[41] D. Menshykau, R.G. Compton, Electroanalysis.. 20(22) (2008) 2387–2394.
[42] Y. Reda, R. Abdel-Karim, K.M. Zohdy, S. El-Raghy, Ain Shams Engineering Journal 13 (2022) 101532.
[43] Y. Reda, H. M.Yehia, A. M.El-Shamy, Egyptian Journal of Petroleum 31 (2022) 9–13
[44] K. M. Zohdy, R. M. El-Sherif, A. M. El-Shamy, Journal of Bio- and Tribo-Corrosion 7(2) (2021) 1-7.